Lennard-Jones interaction parameters of Mo and W in He and N2 from collision cross-sections of Lindqvist and Keggin polyoxometalate anions

Sébastien Hupin, Vincent Tognetti, Frédéric Rosu, Séverine Renaudineau, Anna Proust, Guillaume Izzet, Valérie Gabelica, Carlos Afonso, Hélène Lavanant

Lennard-Jones interaction parameters of Mo and W in He and N_2 from collision cross sections of Lindqvist and Keggin polyoxometalate anions

Sébastien Hupin,[a] Vincent Tognetti, [a] Frédéric Rosu, [b] Séverine Renaudineau, [c] Anna Proust, [c] Guillaume Izzet, [c] Valérie Gabelica, [d] Carlos Afonso, [a] Hélène Lavanant [a] *

ABSTRACT: Drift tube ion mobility spectrometry (DTIMS) coupled with mass spectrometry was used to determine the collision cross sections (^{DT}CCS) of polyoxometalate anions in helium and nitrogen. As the geometry of the ion, more than its mass, determines the collision cross section with a given drift gas molecule, we found both Lindqvist ions $Mo_6O_{19}^{2-}$ and $W_6O_{19}^{2-}$ had $^{DT}CCS_{He}$ values of 103 ± 2 Å^2, and both Keggin ions $PMo_{12}O_{40}^{3-}$ and $PW_{12}O_{40}^{3-}$ had a $^{DT}CCS_{He}$ values of 170 ±2 Å^2. Similarly, ion mobility experiments in N_2 led to $^{DT}CCS_{N2}$ values of 223 ± 2 Å^2 and 339 ± 4 Å^2 for Lindqvist and Keggin anions, respectively. Using optimized structures and partial charges determined from density functional theory calculations, followed by CCS calculations with the trajectory method, we determined Lennard Jones 6-12 potential parameters ε, σ of 5.60 meV, 3.50 Å and 3.75 meV, 4.40 Å for both Mo and W atoms interacting with He and N_2, respectively. These parameters reproduced the CCS of polyoxometalates within 2% accuracy.

INTRODUCTION

Polyoxometalates (POMs) are oxo-clusters constituted of multiple MO_x polyhedra incorporating a metal atom M from the transition metal group 5 or 6 (such as Mo^{VI} or W^{VI}) sharing O atoms. POMs adopt very diverse structures, among which several structural motifs recur. Lindqvist (or hexametalates), decametalates are isopolynanions. Keggin or Dawson ions are heteropolyanions that incorporate tetrahedrally-coordinated heteroatoms (*e. g.* P or Si) in their structures (Figure 1).[1-3]

Mass spectrometry (MS) with electrospray ionization (ESI) is a powerful tool for the analysis of POM compounds,[4-6] particularly for characterizing large POM-based assemblies.[7-9] In the last decade, ion mobility spectrometry (IMS) has been coupled to mass spectrometry (MS) to further characterize POM anions and assemblies.[10-14] Thiel *et al.* observed in 2011 the self-assembly of a hybrid POMs by traveling wave ion mobility spectrometry (TWIMS).[14] Izzet *et al.* in 2015 showed the formation of POM self-assembling in the presence of palladium with a TWIM-MS device.[12] Ion mobility spectrometry enables separating ions of similar *m/z* and determining collision cross sections (CCS), which depend on the size and shape of the ions. However, with TWIMS, a CCS estimation requires a calibration with compounds of CCS values previously measured with drift tube ion mobility spectrometers (DTIMS).[15] In the negative ion mode, available calibrants with drift tube CCS values determined in helium ($^{DT}CCS_{He}$) or nitrogen ($^{DT}CCS_{N2}$) include singly charged ions,[16] poly-DL-alanine, polymalic acid,[17] dextran,[18] lipids,[19] oligonucleotides,[20, 21] deprotonated proteins,[22] and phosphoric acid cluster ions.[23] However, POMs are comparatively denser, and usually multiply charged. POMs are also remarkable because their structures are similar for atoms of very different masses (Mo: 96 u and W: 184 u).

Collision cross sections values in helium $^{DT}CCS_{He}$ of several POMs have been reported by Surman *et al.* in 2016.[10] They have measured $^{DT}CCS_{He}$ for anions derived from four POM salts with tetrabutylammonium (TBA^+ or $C_{16}H_{36}N^+$): two Mn-Anderson derivatives $(TBA)_3[MnMo_6O_{24}(C_4H_8N)_2]$ and $(TBA)_3[MnMo_6O_{24}(C_{20}H_{38}NO)_2]$, a Keggin POM $(TBA)_3[PW_{12}O_{40}]$) and a Dawson POM $TBA_{)6}[P_2W_{18}O_{62}]$). In 2019, Marianski *et al.*[13] reported $^{DT}CCS_{He}$ values of several molybdenum oxide nanoclusters. Our group has also presented collision cross section in N_2, $^{DT}CCS_{N2}$ values obtained from a series of standards polyoxometalate bare anions and clusters formed with their TBA^+ counter ion. In 2018, we presented 45 $^{DT}CCS_{N2}$ values at 30°C or 60°C measured on a DTIMS and showed these values could be used to calibrate a TWIMS device.[11]

Experimentally determined collision cross section can be compared to calculated CCS values determined from tridimensional structures. Computational chemistry and collision cross sections calculations are here needed to deduce geometry information from the collision cross section measurements. Density functional theory (DFT) successfully describes cluster and oxide models.[24-27] Collision cross sections can be then calculated with different methods: the projection approximation method (PA),[28] the

[a.] Normandie Univ, UNIROUEN, INSA Rouen, CNRS, COBRA, 76000 Rouen, France
[b.] CNRS, University of Bordeaux and INSERM, Institut Européen de Chimie et Biologie (IECB, UMS3033, US001), 2 rue Robert Escarpit, 33600 Pessac, France
[g.] Sorbonne Universités, UPMC Univ Paris 06, CNRS UMR 8232, Institut Parisien de Chimie Moléculaire, 4 Place Jussieu, F-75005 Paris, France
[d.] University of Bordeaux, INSERM and CNRS, Laboratoire Acides Nucléiques: Régulations Naturelle et Artificielle (ARNA, U1212, UMR5320), site IECB, 2 rue Robert Escarpit, 33600 Pessac, France
Corresponding author helene.lavanant@univ-rouen.fr
Electronic Supplementary Information (ESI) available

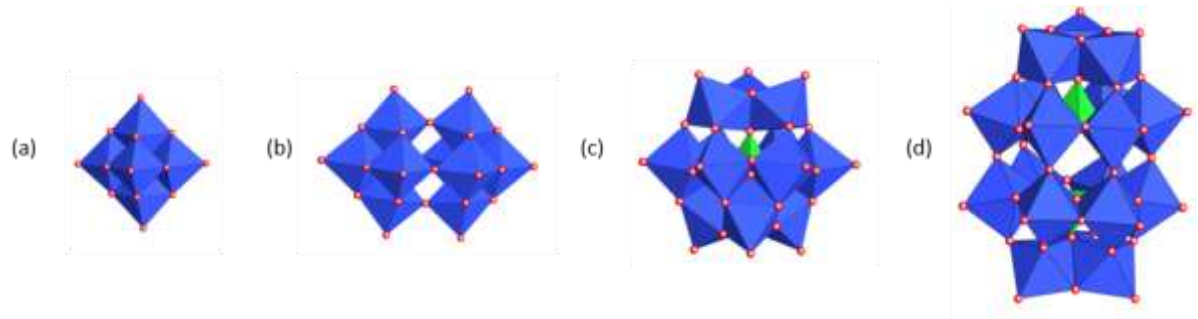

Figure 1. Representations of the four POM structures studied herein. Metal oxide units are represented as blue polyhedra with metal atoms inside and oxygen atoms outside. The green polyhedral represents the tetrahedrally-coordinated heteroatom. (A) Lindqvist structure, (B) Decatungstate Structure, (C) Keggin structure, (D) Dawson structure

projected superposition approximation (PSA),[29] the exact hard sphere scattering method (EHSS)[30] and the trajectory method (TJ).[31] These latter EHSS and TJ methods, which consider strictly elastic collisions between the ion and buffer gas molecules, have been adapted to include energy accommodation by C. Larriba-Andaluz and C. Hogan[32] and named diffuse hard sphere scattering method (DHSS) and diffuse trajectory method (DTM).

The trajectory method remains the gold standard because it considers the polarizability of the gas and the partial atomic charges on the ion through ion-induced dipole and ion-quadrupole interactions

In particular, the trajectory method is the most realistic estimation of CCS in nitrogen gas because N_2 has a much higher polarizability than He (1.71 Å^3 compared to 0.208 Å^3 for He). The trajectory method includes long-range interaction potential by using a 6-12 Lennard-Jones (LJ) potential, ion-quadrupole and ion-induced dipole potentials. LJ potential parameters ε (well depth) and σ (the distance where the potential becomes positive or x intercept) have been optimized to reproduce experimental CCS of ions derived from organic molecules and fullerenes and are only available for a limited range of atoms, including H, C, N, and O.[33-35] To our knowledge, no parameters exist yet to describe Mo or W, or any other transition metal atom, in interaction with He or N_2, thus limiting the possibility for structural inferences for potentially new POMs and assemblies from IMS.

Here we used DTIMS in helium and nitrogen to determine the collision cross sections of bare POM anions and clusters involving POM anions and one or more counterions (TBA^+, H^+) derived from the four typical structural motifs, Lindqvist (or hexametalates), decametalates, Keggin and Dawson ions comprising either Mo^{VI} or W^{VI} atoms. To enable the comparison of experimental CCS values with theoretical ones, we used two well characterized Lindqvist and Keggin polyanions with Mo^{VI} or W^{VI} atoms, calculated collision cross sections with the trajectory method, and determined LJ parameters for Mo^{VI} or W^{VI} interaction with He and N_2 adapted to our ^{DT}CCS values.

Experimental Section

Materials

Six polyoxometalates as tetrabutylammonium (TBA) salts ($TBA_2Mo_6O_{19}$; $TBA_4W_{10}O_{32}$; $TBA_3PMo_{12}O_{40}$; $TBA_3PW_{12}O_{40}$; $TBA_6P_2W_{18}O_{62}$; $TBA_9P_2Nb_3W_{15}O_{62}$) were synthesized using reported synthetic procedures.[36-39] Acetonitrile was purchased as LC-MS grade from VWR. The six tetrabutylammonium polyoxometalates were dissolved separately in pure acetonitrile to a concentration of 10^{-5} M. A solution with the six mixed POMs was also prepared in pure acetonitrile at the same concentration of 10^{-5} M.

Drift tube ion mobility mass spectrometry measurements

Uniform electric field drift tube ion mobility mass spectrometry (DTIMS-MS) measurements were performed and replicated with an interval of two years, on an Agilent 6560 (Santa Clara, CA). The instrument couples a drift tube to a quadrupole time-of-flight mass spectrometer (IMS-QTOF); it has been described in detail elsewhere.[40]

The samples were directly infused at a flow rate of 4 µL min^{-1} in an electrospray ionization source (ESI) operated in the negative ion mode. The generated anions were transmitted and accumulated by two stages of ion funnels and separated in a drift tube with a length of 78.1 ± 0.2 cm. The standard uncertainty on the length takes into account the possible edge effects of the electric field. This was estimated from the study by Stow *et al.* which determined the effective length of three other Agilent 6560 DTIMS instruments operated in N_2 and under higher voltages to be 78.24 ± 0.16 cm.[41]

Ion mobility separations were performed using helium (He) or nitrogen (N_2) as buffer (or drift) gas. An in-house modification to the pumping system, where a second Tri-scroll 800 pump (Agilent) was connected to the source region (with an Edwards

SP16K connected to the front pumping line), while the original Tri-scroll 800 pump connected to the Q-TOF region, allows faster (a few minutes) equilibration of the pressures. This additional pump ensured appropriate pressure differentials on either side of the drift tube so that the drift gas did not to become mixed with air or argon. For the helium measurements, the pressures were set to 3.75 Torr in the drift tube and 3.57 Torr in the trapping funnel before the flow controller was turned on. We found that adjusting the helium pressure differential with the mass flow controller active was not robust enough to ensure 100% helium in the drift tube. For nitrogen measurements, this is not as critical but the same procedure was applied nevertheless and the pressures were set to similar values. For all measurements, when the flow controller was turned on, the pressure of the gas in the drift tube was 3.89 ± 0.01 Torr (measured using an Agilent CDG-500 capacitance diaphragm gauge), and 3.75 ± 0.01 Torr in the trapping funnel. The correct gas flow and pressure difference in these regions were maintained through a feedback system (640B, MKS Instruments) based on the IMS pressure measured at the rear of the drift tube. The instrument was operated, with covers open, in a well air-conditioned room and the temperature of the drift cell was monitored by a K-type thermocouple (Omega Engineering). The temperature was 296.0 K with a reported standard deviation of 0.5 K.

In order to probe the influence of different experimental conditions on ion mobility and CCS determination, several different sets of parameters where used which are listed in table S1 (in the electronic supplementary information). Among the parameters varied were the voltage applied on the Agilent-named optics 1 or fragmentor, and the voltages applied in the rear funnel and transfer optics to the QTOF analyser. The optics 1 or fragmentor voltage corresponds to the part of the ESI source that speeds up ions from the glass capillary to the high pressure funnel resulting in one of the principal cause of in-source collision induced dissociation (in-source CID). Fragmentor voltages leading to soft or harsh desolvation and in-source CID were used. All other parameters, like the trap entrance grid delta, the trap fill time and trap release time were set to the values chosen from a previous study[42] which aimed at ensuring a soft transmission in the trapping funnel before the ion mobility drift tube. For the post-IMS transmission, we used the default setting and two experimental tunings described thoroughly by Gabelica *et al.*[42] that were obtained using the ammonium-bound bimolecular G-quadruplex, which easily undergoes ammonia loss. These tunings consist in different gradients of DC voltages between the exit of the ion mobility cell and the TOF analyser. We will refer these post ion mobility settings as "standard", "compromised" and "optimized", depending on how steep or mild slope of the voltage gradient.

To obtain the reduced mobility values (K_0) and determine CCS values, we used the stepped field (also called multi-field) method. The five to ten values of the electric field were applied in the drift tube for 1 to 2 min each. The applied electric field ranged between 5 and 10 V/cm, for helium, and 7 to 19 V/cm in nitrogen. Taking the pressure and temperature into account, the gas number density N was 1.26 10^{23} m^{-3}, and this amounted to reduced electric field strengths (E/N) of 4 to 8 Td for helium and 6 to 15 Td in nitrogen.

Data analysis

The ion mobility spectra acquired by the Agilent instrument were visualized by the Agilent IM-MS browser (version B.08.00, build 8.0.815.0) and extracted with the MIDAC_CIU_Extractor from the CIUSuite 2 developped by Polaski *et al*.[43] The time values (t) obtained from the extracted ion mobility spectra (EIM) (also called arrival time distributions (ATD)) were collected, smoothed with the Savitzky-Golay method (window-size 1 ms) and the center of the peak were picked at 75% picking height, using mMass (5.5.0) [44, 45]. Classical linear regression based on least squares minimization of time vs. the reciprocal of the field strength ($1/E$) at different electric fields were performed in OriginPro 2018 (version b.9.5.0.193) or in a Microsoft Excel spreadsheet (2016 MSO 16.0.4266.1001 64 bits).

The least square linear fit allowed to retrieve, from the intercept, the time spent by the ions outside the drift cell (t_0) and the slope from which the value of the ion mobility (K) was inferred, according to Eq.1.

$$t = \left(\frac{L}{K}\right) \cdot \frac{1}{E} + t_0 \qquad (1)$$

We will refer to t as the drift time, although it is often called arrival time because of the non-null value of t_0. We obtained the linear regressions of five to ten points with standard error values on the slope and intercept.

The K values were then converted to a reduced ion mobility K_0 to scale the ion mobility into the gas number density value N_0 at standard pressure and temperature (N_0, p_0 and T_0, 2.687 10^{25} m^{-3}, 760 Torr and 273.15 K, respectively) (Eq. 2). We determined the ^{DT}CCS values in He or N_2 using the low-field limit equation (Eq. 3) where e is the elementary charge, k_B the Boltzmann constant, z the charge number, μ the reduced mass of the ion and the drift gas and T_{eff} is the effective temperature calculated from Eq. 4 where M is the mass of the drift gas.[46] Effective temperature was calculated at the mean field strength. Note the use of effective temperature increases the temperature compared to the room temperature measured (296.0 K) and decreases the CCS values, all the more so at high electric fields. As a

range of electric fields are applied, the value chosen (301 K) is necessarily an approximate value.

$$K_0 = \frac{N}{N_0}K = \frac{p}{p_0}\frac{T_0}{T}K \qquad (2)$$

$$^{DT}CCS = \frac{\sqrt{18\pi}}{16}\frac{e}{\sqrt{k_B T_{eff}}}\frac{z}{\sqrt{\mu}}\frac{1}{N_0}\frac{1}{K_0} \qquad (3)$$

$$T_{eff} = T + \frac{M(KE)^2}{3k_B} \qquad (4)$$

Computational details

Crystal structures were obtained from the Cambridge Crystallographic Data Centre (CCDC) for $TBA_2Mo_6O_{19}$,[47] (CCDC 831885), $TBA_2W_6O_{19}$,[48] (CCDC 1267643), $TBA_3PMo_{12}O_{40}$ (CCDC 647440)[49] and $TBA_3PW_{12}O_{40}$ (CCDC 891265)[50, 51]. The coordinates of the POM anions without TBA^+ were extracted and used in quantum chemistry (QC) calculations.

Gas phase QC calculations were carried out within Kohn-Sham DFT using the Gaussian09 software,[52] the dispersion-corrected range-separated hybrid ωB97X-D exchange-correlation functional.[53] The 6-31G(d) all-electron basis set was used for all non-metallic atoms, while Mo and W were described by the standard SDD pseudopotential in conjunction with the associated valence basis set. The QC calculations were also used to calculate atomic partial charges fitted to the electrostatic potential using the Hu-Lu-Yang model with Gaussian's standard atomic densities (referred as HLYGAt atomic charges).[54]

Cross section calculations were carried out using MOBCAL [30, 31] and IMOS 1.10. [55, 56]

The trajectory method in MOBCAL were carried out with in both helium (mass 4.0026 u and polarizability 0.205 10^{-30} m^3) and nitrogen gas (mass 28.01 u and polarizability 1.71 10^{-30} m^3). The HLYGAt atomic charges were used in the trajectory method CCS calculations. The LJ value for oxygen or phosphorus were from Campuzano et al.[33] or directly from the MOBCAL code. The number of trajectories was set (number of complete cycles (itn) 10, number of velocity points (inp) 20-40 , number of random points (imp) 500-1000, total number of points 100 000-400 000) so that standard deviations on the trajectory method were 2% or less.

In order for the calculations in IMOS 1.10 to be comparable to MOBCAL, the trajectory method with fully elastic collisions was used (no accommodation coefficient was used: it was set to 0),and the LJ parameters of P and O were set to the values used in our MOBCAL calculations. In N_2, the ion quadrupole interaction was used. The number of orientations was left at 3 and the number of gas molecules per orientation was set from 100 000 to 300 000. The timestep coefficient was set to 100 or 150. All calculations were performed at a temperature of 301 K. Precursor ions that fragment in the transmission area between the drift tube and the TOF analyzer are frequent in ion mobility mass spectrometry of cluster or aggregated ions and complicate the attribution of ion mobility signals.[57-61] Figures S1-S7 in the supplementary information show the mass spectra, the extracted ion mobility spectra and the $^{DT}CCS_{He}$ of all studied ions. The extracted ion mobility spectra exhibited several peaks for nearly all the ions because precursor ions could be present but also because, in some cases like for $[PMo_{12}O_{40} + TBA]^{2-}$, ions of neighboring *m/z* values were present. Indeed, the width of the isotopic distribution caused an overlapping of mass spectrometric signals especially when a mixture of POM salts was used. Nevertheless, the most intense signals, present in all experimental conditions and for the five different drift field values were used to determine $^{DT}CCS_{He}$ values. The graph on Figure 2c and 2e show all the $^{DT}CCS_{He}$ values obtained with the different experimental conditions. Variations in the resulting $^{DT}CCS_{He}$ values were observed depending on experimental settings, but no systematic tendency could be discerned when comparing the results of the different experimental conditions for all ions (Figure S1-S7). We therefore hypothesized that all errors were random and calculated the mean CCS value and standard deviation using all measurements (Table 1). Standard deviations ranged from 0.5 to 4.8 $Å^2$, which amounted to relative standard deviation of 0.4 to 1.4%, which is in the range of what has been previously reported.[21, 41] Note that these values were obtained using four to seven replicates. The number of replicates were lower for $[PMo_{12}O_{40}]^{3-}$, $[P_2W_{18}O_{62} + 2\ TBA]^{4-}$ because these ions, more labile, were not observed when higher voltages were applied to the fragmentor.

Results and discussion

The negative ion ESI mass spectra of polyoxometalate salts solutions in acetonitrile presented signals from bare POM ions and clusters of these POM ions with TBA cations or protons resulting in lower charge cluster ions.[11] In fact, bare POM ions were present only for smaller and lower charge POMs, such as Lindqvist, and Keggin POM ions. Larger and more highly charged decatungstate and Dawson structures appeared only as cluster ions with TBA cations or protons. A number of fragment ions also appeared, among which are clusters with butyl $C_4H_9^+$ counter-ions and smaller metal oxyanions. These ions were observed from pure POM solutions as well as mixtures of POM salts. $W_6O_{19}^{2-}$ was one of the major fragment ions observed in the mass spectra obtained from $TBA_4W_{10}O_{32}$. In addition to these four ions, we included eleven different cluster ions with TBA and proton counter ions, six of which have been studied by Surman et al. [10] (Table 1).

Ion mobility in helium

Figure 2 displays the isotopic distribution, the extracted ion mobility spectra and the $^{DT}CCS_{He}$ determined with the multi-field method of two Linqvist POMs $Mo_6O_{19}^{2-}$ and $W_6O_{19}^{2-}$. The mass spectra in Figure 2a and 2d were obtained from a solution of the six mixed POM salts salts with low fragmentor voltage and optimized post IMS tuning. The ion mobility spectra were extracted across the entire isotopic distribution. Extracting the entire distribution rather than one single isotopic peak did not change the ion mobility profiles but led to signals of higher intensity. For each field (only 7.553 V cm^{-1} is shown on Figure 2), the ion mobility signals presented different drift times, widths and profiles depending on the experimental conditions in the ion source (soft harsher fragmentor voltages are represented by light or darker colors respectively) and in the post IMS transfer area (standard transmission (green traces) , compromised (orange, red and brown traces) and optimized (blue traces) post IMS settings as described in Table S1). The shallower voltage gradients associated with the compromised and optimized post IMS settings resulted in longer drift times which could clearly be attributed to longer t_0 (time spent by the ions outside the drift cell) and thus did not result in any significant difference in ^{DT}CCS values. Across all experimental conditions, the resolution calculated from the full width at half maximum (FWHM) varied from 8 to 19 and peak widths and profiles were comparable with several differences. For $Mo_6O_{19}^{2-}$, harsher fragmentor voltages led to a single narrow peak (most visible in the dark green trace in Figure 2b) and resulted in $^{DT}CCS_{He}$ values smaller by 1-2 $Å^2$, which we did not regard as a significant difference. Because of a lower resolution, the effect of the fragmentor voltage on peak width was less apparent in the compromised and optimized settings for which the resolution was around 10. For $W_6O_{19}^{2-}$, additional peaks before the main signal that were only present when low fragmentor voltages were applied (light green, orange, red and light blue traces in Figure 2d). Rather than different conformations, highly unlikely for the very stable Lindqvist structures, these additional signals should be attributed to larger or more highly charged precursor ions that fragment in the transmission area between the drift tube and the TOF analyser to give the Lindqvist anions. When shallow voltages gradients are applied in the source area, the lower energy of the collisions with residual gas molecules, in this intermediate pressure area of the ion source, might not be sufficient to achieve complete desolvation or declustering.

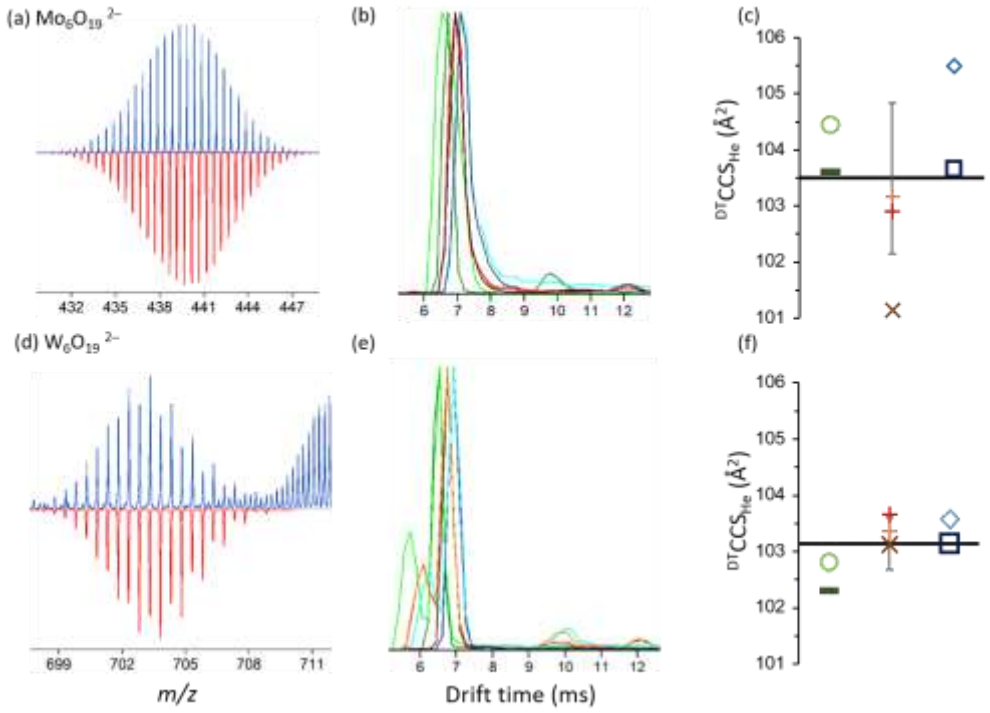

Figure 2. (a) and (d) Isotopic distribution of the $Mo_6O_{19}^{2-}$ (*m/z* 439.8) and the $W_6O_{19}^{2-}$ (*m/z* 703.5) Lindqvist POM anions with the experimental mass spectrum in blue blue (soft fragmentor voltage and optimized post IMS tuning) and the calculated distribution in red. (b) and (e) Extracted ion mobility spectra for the distribution around *m/z* 439.8 or *m/z* 703.5 at 7.553 V cm^{-1} with seven different experimental conditions. (c) and (f) $^{DT}CCS_{He}$ of the $Mo_6O_{19}^{2-}$ or the $W_6O_{19}^{2-}$ Lindqvist POM anions obtained from the seven different experimental conditions. The mean values are represented by a black horizontal line and the vertical error bars represent the standard deviation. Legend of experimental conditions in (b), (c) (e) and (f): green (dash and circle): standard post IMS tuning; blue (square and diamonds): compromised post IMS tuning; orange, red and brown (crosses): optimized post IMS tuning; dark green, brown and dark blue were obtained with harsh fragmentor voltages, and light colors with soft fragmentor voltages.

Ions with residual solvent molecules could be present which would not be expected to survive across the drift tube and on to the QTOF analyser, as they are very weakly bound. The presence of residual clusters with solvent molecules could contribute to longer drift times and affect peak widths. Thus, the presence of adducted precursor ions affected the ion mobility profile when low fragmentor voltages were applied. This interpretation was confirmed by the fact that these signals, attributed to precursor ions, were less intense when harsher fragmentor voltages were used.

Values of $^{DT}CCS_{He}$ of the Lindqvist anions $[Mo_6O_{19}]^{2-}$ and $[W_6O_{19}]^{2-}$ were found to be very close (103.7 and 103.3 Å^2) and consistent with the value of 102 Å^2 obtained by Marianski et al.[13] It was indeed expected that the values of $^{DT}CCS_{He}$ would be close for the two Lindqvist anions since their structures are nearly identical. The fact that similar values of $^{DT}CCS_{He}$ were obtained with anions of widely different *m/z* values is nevertheless remarkable compared to previously reported CCS which usually show a dependence of CCS on the mass and depending on the molecular class.[16] The anions of the Agilent ESI-L tuning mix *m/z* 602, 1034, 1334, 1634, have a ratio of mass over CCS that range from 5.1 to 6.7 Da Å^{-2} for $^{DT}CCS_{He}$ values.[21] As a comparison, the ratio of mass over CCS for the Lindqvist anions were here calculated to be 8.48 and 13.6 Da Å^{-2} for Mo and W containing structures respectively. Note that for such compact, and high ion mobility ions, effective temperature can be up to 7.5 K higher than the room temperature measured at 296.0 K, for an electric field at 10.1 V cm^{-1}. Using effective temperature in the Mason-Schamp equation rather than ambient temperature led to a decrease of $^{DT}CCS_{He}$ value of 0.5 to 1.5 Å^2. The values reported here were calculated with the effective temperature at an electric field of 7.56 V cm^{-1} which was 5 K above room temperature (301 K). Marianski et al. [13] reported measurements at 10 to 15 V cm^{-1}, the effective temperature should therefore be higher, consistent with a lower $^{DT}CCS_{He}$ value.

The $^{DT}CCS_{He}$ values of Keggin anions $[PMo_{12}O_{40}]^{3-}$ and $[PW_{12}O_{40}]^{3-}$ were also very similar, respectively 170.1 and 170.9 Å^2. Here the value of $^{DT}CCS_{He}$ of $[PW_{12}O_{40}]^{3-}$ was 21 Å^2 larger than the value published by Surman et al.[10] A similar discrepancy of 17 Å^2 was observed for the cluster ion $[PW_{12}O_{40} + TBA]^{3-}$ and differences of 8 to 14 Å^2 were obtained for Dawson cluster anions $[P_2W_{18}O_{62} + 2\ TBA]^{4-}$, $[P_2W_{18}O_{62} + 2\ TBA + H]^{3-}$ and $[P_2W_{18}O_{62} + 3\ TBA]^{3-}$. Conversely, we obtained a $^{DT}CCS_{He}$ value for the $[P_2W_{18}O_{62} + 4\ TBA]^{2-}$ Dawson cluster anion 15 Å^2 lower than the previously published value. [10]

Dawson anions could only be observed as clusters with TBA counter ions, their structures are therefore not well characterised compared to bare POM anions and could present different conformations. We nevertheless observed that ions of similar numbers of TBA counter ions had neighboring $^{DT}CCS_{He}$ values. Dawson anions with two TBA counter ions, $[P_2W_{18}O_{62} + 2\ TBA]^{4-}$, $[P_2W_{18}O_{62} + 2\ TBA + H]^{3-}$, $[P_2Nb_3W_{15}O_{62} + 2\ TBA + 3\ H]^{4-}$ and $[P_2Nb_3W_{15}O_{62} + 2\ TBA + 4\ H]^{3-}$ had $^{DT}CCS_{He}$ values between 321.3 and 330.1 Å^2 with slightly higher values for higher charged 4– ions. Dawson anions with three TBA counter ions, $[P_2W_{18}O_{62} + 3\ TBA]^{4-}$ and $[P_2Nb_3W_{15}O_{62} + 3\ TBA + 3\ H]^{3-}$, had $^{DT}CCS_{He}$ values of 365.3 and 367.0 Å^2. Expectedly, the $^{DT}CCS_{He}$ values increased with the number of TBA, by 30 to 50 Å^2 depending on the ion and charge state.

Several anions, especially among the highly charged anions were only visible with low fragmentor voltages, i.e. soft ion transmission. Among these highly charged anions $[P_2W_{18}O_{62} + 2\ TBA]^{4-}$, $[P_2Nb_3W_{15}O_{62}+2TBA+3H]^{4-}$, but also $[PMo_{12}O_{40}]^{3-}$ were included in table 1, as their $^{DT}CCS_{He}$ values were consistent with different instrumental conditions (Figure S3, Figure S5). We chose not to include $[W_{10}O_{32}]^{4-}$ as its $^{DT}CCS_{He}$ values were not consistent across different experimental conditions (Figure S8). This was surprising from a bare POM anion with an expected rigid geometry. The presence of residual solvent molecules or adducted precursor ions that fragment in the ion mobilty drift tube could explain this variation in $^{DT}CCS_{He}$.

Ion mobility in nitrogen gas

In 2019, we had used two sets of experiments obtained on a TOFWerk DTIMS-TOF instrument to determine the $^{DT}CCS_{N_2}$ values of 45 ions derived from POM anions.[23] The TOFWerk DTIMS-TOF instrument was operated at a high pressure (1 bar) and high electric fields (300-450 V cm^{-1}). The resulting reduced electric fields were 1 to 2 Td.

Here we wanted to determine $^{DT}CCS_{N_2}$ values on the Agilent 6560 DTIMS which operates at lower pressure, lower electric fields but higher reduced electric fields. We used a set of ten values for the electric fields to bring reduced fields to values between 6 and 15 Td and thus reach values comparable to the experiments in helium. Assessing the linearity of the multi-field method over a larger range and lower electric field values was also an objective.

Figure 3 shows the extracted ion mobility profiles of the Lindqvist anion $[Mo_6O_{19}]^{2-}$ at *m/z* 439.8 at ten values of electric fields ranging from 19.08 to 7.56 V cm^{-1}, the graph of drift times vs the reciprocal of the electric field (1/E) and the residues resulting from the linear fit of the data obtained from the peaks of the extracted ion mobility spectra at *m/z* 439.8.

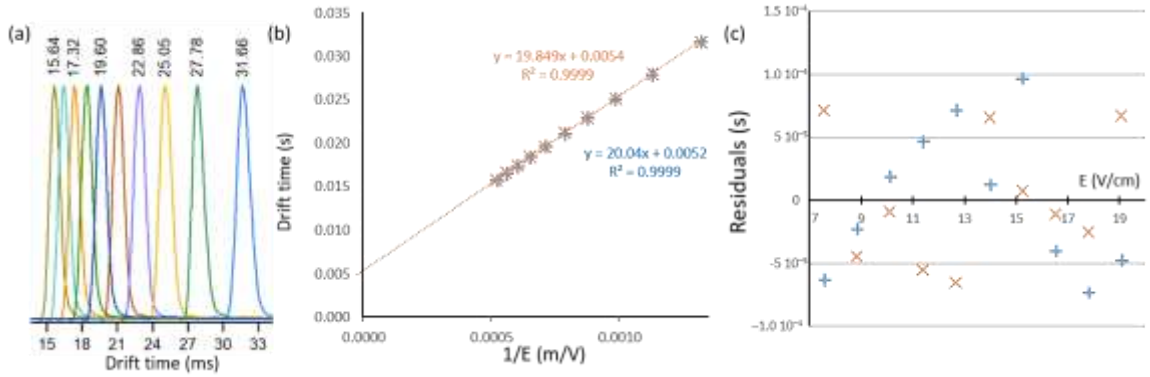

Figure **3.** (a) Overlay of the extracted ion mobility spectra of Lindqvist anion $[Mo_6O_{19}]^{2-}$ at *m/z* 439.8 at ten values of electric fields ranging from 19.08 to 7.56 V cm^{-1}. The displayed data were obtained with a harsh fragmentor voltage of 450 V and the "compromised" post IMS tuning. (b) Linear fit of the drift time *vs* the reciprocal of the electric field for $[Mo_6O_{19}]^{2-}$anions. (c) Residuals of the linear fit. Soft fragmentor voltage: orange diagonal crosses and harsh fragmentor voltage: blue vertical crosses.

Expectedly, the resolution and the peak width increased with lower electric field values: FWHM values changed from 1.0 to 1.3 ms as the field decreased from 19.08 to 7.56 V cm^{-1}. This was expected from the longer time spent in the ion mobility cell that caused broadening of the ion packet. The drift time remained very well correlated to the reciprocal of the electric field down to lower electric field values (*i.e.* up to higher 1/E) and the residuals calculated from the fitted data for $[Mo_6O_{19}]^{2-}$ anions showed no systematic error.

Similar results were observed for all the POM ions observed (Figure S9-S21). When multiple peaks were observed in the extracted ion mobility spectra, we attributed the signals of the targeted POM anions by selecting peaks that were visible both with soft and harsh fragmentor voltages and for all ten values of electric fields. Values obtained from the mean of the two values obtained with soft and harsh fragmentor voltages and the "compromised" post IMS tuning are collected in Table 1.

Focusing on the bare POM anions $[Mo_6O_{19}]^{2-}$, $[W_6O_{19}]^{2-}$, $[PMo_{12}O_{40}]^{3-}$ and $[PW_{12}O_{40}]^{3-}$, we expectedly obtained similar $^{DT}CCS_{N2}$ values of 223.2 and 223.7 $Å^2$ for the two Lindqvist structures and 340.1 and 337.2 $Å^2$ for the two Keggin anions. These values are comparable to the values obtained in 2019, which were 220, 343 and 337 $Å^2$, and within an error of less than 2 %. The $^{DT}CCS_{N2}$ values of clusters of POM ions with TBA cations were much more different, with systematically lower values obtained here on the Agilent instrument compared to the $^{DT}CCS_{N2}$ values obtained in 2019 on the TOFWerk instrument. Discrepancies ranged from 9 to 24 $Å^2$ amounting to 2 to 4 % differences. Conformations of these clusters of POM ions with TBA cations could depend more on experimental conditions, both in the ion source and the drift tube. It is therefore difficult to draw any conclusion. Surprisingly, the $^{DT}CCS_{N2}$ values of Keggin anions were very similar for both bare triply charge anions, and doubly charged anions with one TBA counter ion (from 337.2 and 340.2 $Å^2$).

We also observed, however, that for Dawson POMs with similar charge states and number of TBA counter ions, such as Dawson POMs with two or three TBA counter ions, the $^{DT}CCS_{N2}$ values depended more strongly on the charge state than the $^{DT}CCS_{He}$ values: Dawson POMs with two TBA counter ions had $^{DT}CCS_{N2}$ values around 528 $Å^2$ with 4– charge states, and values around 468 $Å^2$ for 3– charge states. As a consequence, Dawson POMs with three TBA counter ions and 3– charge states had lower $^{DT}CCS_{N2}$ values (503.3 and 506.5 $Å^2$) than Dawson POMs with two TBA counter ions and 4– charge states. The same tendency, but with $^{DT}CCS_{N2}$ values 9 to 24 $Å^2$ higher, had been observed in the values obtained on the TOFWerk IMS-TOF instrument.[23]

When seeking for correlations between $^{DT}CCS_{N2}$ and $^{DT}CCS_{He}$ values, it appeared clearly that the correlation depended on charge state (Figure 4): linear correlations with determination coefficients higher than 0.999 could be obtained from doubly and triply charged ions. When reduced ion mobilities in He and N_2 were compared, a correlation with a second order polynomial was the better fit for doubly and triply charged ions (Figure 4b) which is consistent with equation (3) where the reduced ion mobility K_0 is inversely proportional to the CCS.

The POM ions being both highly charged and polar, the ion-induced dipole and ion-quadrupole interactions are expected to play a large role, all the more so in nitrogen gas because N_2 has a much higher polarizability than He. The difference in slope with different charge states emphasized the fact that any CCS calculation method used for these systems

Table 1. Reduced ion mobility K_0 and collision cross sections ^{DT}CCS in helium and nitrogen of fifteen ions and clusters with tetrabutylammonium for Lindqvist, decatungstate, Keggin and Dawson polyoxometalates at an average effective temperature of 301 K and a mean field value of 6.0 Td in He, and 10.5 Td in N_2 . The numbers in parenthesis are the standard deviations (SD);); n is the number of replicates. The values in N_2 were obtained with ten values of electric fields, from two measurements with soft and harsh fragmentor voltages except for $[P_2W_{18}O_{62} + 2\ TBA]^{4-}$, $[P_2Nb_3W_{15}O_{62} + 2\ TBA + 3\ H]^{4-}$ and $[P_2Nb_3W_{15}O_{62} + 2\ TBA + 4\ H]^{3-}$ which were only visible with soft fragmentor voltages.

				He						N_2				
Structure	Ion	*z*	*m/z*	K_0(He)	(SD)	$^{DT}CCS_{He}$	(SD)	n	Litterature	$K_0(N_2)$	(SD, *n* = *2*)	$^{DT}CCS_{N2}$	(SD, *n* = 2)	Published[c]
				$cm^2\ V^{-1}\ s^{-1}$		$Å^2$			$Å^2$	$cm^2\ V^{-1}\ s^{-1}$		$Å^2$		$Å^2$
Linqvist	$[Mo_6O_{19}]^{2-}$	2	439.79	10.312	(0.122)	103.7	(1.3)	7	102[a]	1.843	(0.012)	223.2	(1.5)	220
	$[W_6O_{19}]^{2-}$	2	703.52	10.322	(0.049)	103.3	(0.5)	7		1.829	(0.008)	223.7	(1.0)	
	$[Mo_6O_{19} + TBA]^{-}$	1	1122.04	3.167	(0.013)	169.6	(0.6)	7		0.814	(0.004)	252.1	(1.1)	263
Decatunsgtate	$[W_{10}O_{32} + 2\ TBA]^{2-}$	2	1417.66	4.135	(0.037)	259.3	(2.3)	7		1.089	(0.001)	374.2	(0.3)	383
Keggin	$[PMo_{12}O_{40}]^{3-}$	3	607.37	9.422	(0.051)	170.1	(1.2)	4		1.800	(0.021)	340.1	(4.0)	343
	$[PW_{12}O_{40}]^{3-}$	3	959.00	9.370	(0.034)	170.9	(0.7)	7	150[b]	1.810	(0.010)	337.2	(1.8)	337
	$[PMo_{12}O_{40} + TBA]^{2-}$	2	1032.3	4.905	(0.046)	218.8	(2.3)	7		1.201	(0.003)	339.7	(1.0)	348
	$[PW_{12}O_{40} + TBA]^{2-}$	2	1559.76	4.784	(0.015)	224.2	(0.9)	7	207[b]	1.197	(0.002)	340.2	(0.7)	349
Dawson	$[P_2W_{18}O_{62} + 2\ TBA]^{4-}$	4	1212.00	6.510	(0.088)	328.3	(4.7)	4	314[b]	1.544		526.3		550
	$[P_2Nb_3W_{15}O_{62}+2TBA+3H]^{4-}$	4	1144.55	6.478	(0.085)	330.1	(4.6)	4		1.535		529.7		552
	$[P_2W_{18}O_{62} + 2\ TBA + H]^{3-}$	3	1616.30	5.004	(0.069)	321.3	(4.6)	7	310[b]	1.297	(0.006)	470.0	(2.2)	481
	$[P_2Nb_3W_{15}O_{62}+2TBA+4H]^{3-}$	3	1526.41	4.950	(0.049)	325.0	(3.5)	6		1.304		467.7		483
	$[P_2W_{18}O_{62} + 3\ TBA]^{3-}$	3	1696.82	4.398	(0.053)	365.3	(4.2)	7	357[b]	1.212	(0.001)	503.3	(0.1)	520
	$[P_2Nb_3W_{15}O_{62}+3TBA+3H]^{3-}$	3	1606.89	4.384	(0.054)	367.0	(4.8)	6		1.204	(0.005)	506.5	(2.3)	523
	$[P_2W_{18}O_{62} + 4\ TBA]^{2-}$	2	2666.50	2.699	(0.031)	397.3	(4.6)	7	412[b]	0.796	(0.001)	510.9	(0.1)	

a.[13] b.[10] c.[23]

should take the electrostatic interactions into account. Only the methods derived from the trajectory method do so at present.

In all cases, ions of similar expected structures involving different metals (Mo , W or Nb and W) appeared with similar CCS and K_0 values in both gases when identical charge states were compared. This was true in spite of the fact that their *m/z* values differ by up to 60%. The ratio of mass over $^{DT}CCS_{N2}$ values ranged from 3.9 to 10.4 Da Å^{-2}, generally higher than the values from usual calibrants. Indeed mass over $^{DT}CCS_{N2}$ ratios range from 1.5 to 3.3 Da Å^{-2} for polyalanine deprotanated molecules,[17] from 2.0 to 6.3 Da Å^{-2} for dextran derived anions,[18] from 2.0 to 7.4 Da Å^{-2} for phosphoric acid cluster anions.[23]

Collision cross section calculation and determination of Lennard Jones parameters

Geometry optimizations with DFT were carried out with crystal structures as starting points and expectedly the optimized geometries were nearly identical to crystal structures and between Mo and W based POM. Superimposed structures and structural root mean square deviation (RMSD) obtained using the Kabsch alignment algorithm implemented in the VMD software[62] are shown in Figures S22.

DFT calculations also allowed us to calculate atomic partial charges (in elementary charge e units), here in the HLYGAt formalism. The Cartesian coordinates and partial charges of bare Lindqvist and Keggin anions are listed in Tables S2 and S3. The partial charges were 1.8 e for W compared to 1.5 e for Mo for Lindqvist anions, and 1.4 e for W compared to 1.6 e for Mo in Keggin anions. Non-bridging oxygen atoms bore lower partial charges in absolute value (–0.51 e and –0.58 e in $Mo_6O_{19}^{2-}$ and $W_6O_{19}^{2-}$ respectively, –0.47 e and –0.52 e in $PMo_{12}O_{40}^{3-}$ and $PW_{12}O_{40}^{3-}$ respectively) than oxygen atoms bridging two metal atoms that bore partial charges ranging from –0.60 e to –0.71 e.

As recommended in several studies,[33, 34] we used a scaling factor on LJ parameters coming from the universal force field[63] (UFF) to determine LJ parameters for Mo and W atoms. The CCS were calculated with MOBCAL with the trajectory method in He and N_2 for scaling factors ranging from 1 to 1.8 in He and 1.3 to 1.6 in N_2 (figure S23) on the bare Lindqvist anions $Mo_6O_{19}^{2-}$ and $W_6O_{19}^{2-}$. Although the metal atoms are not in an outer position compared to oxygen atoms, the LJ parameters of Mo and W did influence the calculated ^{TJ}CCS values in He and N_2. In fact, $^{TJ}CCS_{He}$ values were doubled when comparing UFF scaling factor of 1.0 and 1.8. The ε and σ values adapted to the $^{DT}CCS(He)$ and $^{DT}CCS(N_2)$ values of this study are listed in Table 2. The UFF scaling factors were found in the same range for Mo and W, around 1.26 for the interactions with He and 1.44 for the interactions with N_2. The resulting proposed LJ parameters are in the same range for Mo and W and are expectedly larger than the LJ parameters of O. As a test of these newly proposed LJ parameters ^{TJ}CCS values were calculated for Keggin anions which yielded 165 and 163 Å^2 for in $PMo_{12}O_{40}^{3-}$ and $PW_{12}O_{40}^{3-}$ respectively in He and 337 and 339 Å^2 in N_2, which are values of 3 to 5 % relative error in He and below 1% in N_2 compared to the experimental values.

To further investigate LJ parameters adapted to the experimental $^{DT}CCS_{He}$ and $^{DT}CCS_{N2}$ values of Lindqvist and Keggin anions, we used the LJ optimizer [64] option available in IMoS 1.10 to explore other possible values of ε and σ values for Mo and W. The results are shown as color surface maps (Figure 5), with a vertical axis and the color accounting for the square root of the $F_{opt,}$ (ε,σ) function (equation 5) which the LJ optimizer calculated. We converted $F_{opt,}$ (ε,σ) values to percentages which amounts to the accumulated relative errors of the calculated CCS values with the trajectory method compared to experimental values of the Lindqvist and Keggin anions.

$$F_{opt}(\varepsilon,\sigma) = \left(1 - \frac{\Omega_{calc}(\varepsilon,\sigma)}{\Omega_{exp}}\right)^2_{Linqvist} + \left(1 - \frac{\Omega_{calc}(\varepsilon,\sigma)}{\Omega_{exp}}\right)^2_{Keggin} \quad (5)$$

The figures 5a-d show as black points and lines the exploration of the surface by use of scaling parameters on UFF LJ parameters corresponding to our MOBCAL calculations. The results show that IMoS calculations agree well with MOBCAL calculations and that these previous MOBCAL calculations did allow to find a local minimum. The optimization surface confirmed that the LJ parameters of Mo and W influenced calculated CCS : relative differences of up 20% (color coded red on the heat maps) are shown. A valley of minima was found, leading to a range of choices for the LJ parameters (emphasized as red dots on figure 5). This has been observed before by Wu et al.[64] who found the intercept σ and well depth ε followed an exponential relation. Here, the line of minima did not show any clear fit, or rather, could follow either linear, second- or third-order polynomials (figure S24). The value of the accumulated relative errors was within 1.1 to 2.8% across this line of minima. Lower accumulated errors were obtained with deeper wells ε and shorter σ values for metal-helium interactions. We chose 5.6 meV and 3.5 Å as LJ parameters for both Mo and W interacting with He because these values give rise to 1.5 % and 2 % accumulated relative errors for Mo and W respectively in IMoS calculations. An input of these proposed LJ parameters in MOBCAL showed these parameters were an improvement compared to our previous scaling: calculated CCS values were within less than 2% relative error for $^{TJ}CCS_{He}$ values (104.3

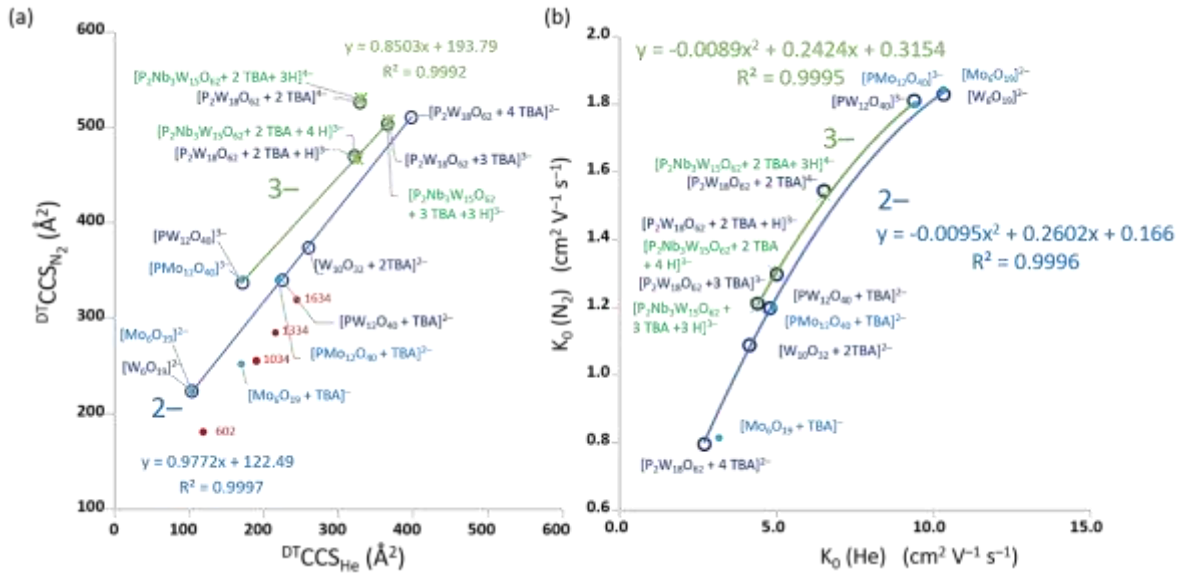

Figure 4. (a) Correlation between $^{DT}CCS_{He}$ values and $^{DT}CCS_{N_2}$ values. (b) Correlation between the reduced ion mobilities $K_0(He)$ and $K_0(N_2)$ of the fifteen POM derived anions . Values for POM with Mo are represented as light blue dots, with W with dark blue circles, with Nb and W with green stars. Red dots show ^{DT}CCS values of singly charged tuning mix anions *m/z* 602, 1034 and 1334, 1634 from Stow et al.[41] and Marchand et al.[21]

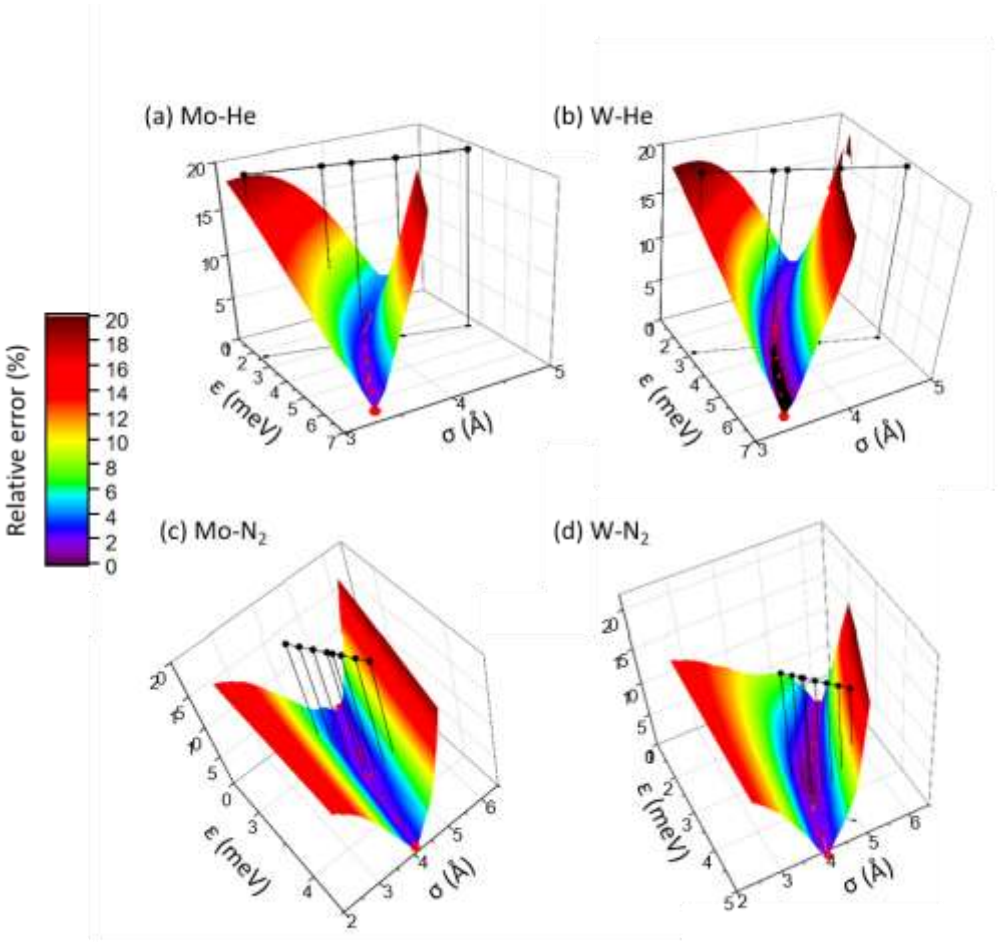

Figure 5. Mapped optimization surface for the ε and σ Lennard Jones parameters (a) for Mo in He (b) W in He, (c) Mo in N_2 and (d) W in N_2. Black points and lines represent the MOBCAL calculations by use of scaling parameters on UFF LJ parameters.

Table 2. Lenard Jones parameters for Mo and W interaction potentials with He and N_2. The Lenard Jones parameters used in all calculations for O and P are also given as found in Campuzano et al[33] or directly from the MOBCAL code.

Atom	O	P	Mo	W	Mo and W
UFF LJ Parameters					
ε (meV)	2.6	1.32	2.4	2.9	
σ (Å)	3.500	4.147	3.052	3.069	
He interaction LJ parameters					
UFF scaling			1.28	1.24	IMoS
ε (meV)	1.07	1.35	3.10	3.60	5.60
σ (Å)	2.43	3.50	3.90	3.80	3.50
N_2 interaction LJ parameters					
UFF scaling			1.47	1.40	IMoS
ε (meV)	2.70	6.31	3.60	4.10	3.75
σ (Å)	3.07	3.47	4.50	4.25	4.40

and 104.7 Å^2 for $Mo_6O_{19}^{2-}$ and $W_6O_{19}^{2-}$ and 167.6 and 168.4 Å^2 for $PMo_{12}O_{40}^{3-}$ and $PW_{12}O_{40}^{3-}$). Accumulated errors showed a clearer minimum in W-N_2 interactions at 3.75 meV and 4.4 Å. These two LJ parameters are associated with an accumulated error of 2% in Mo-N_2 data and could therefore be chosen for Mo-N_2 interactions. When 3.75 meV and 4.4 Å were used as input in MOBCAL calculations, the resulting calculated $^{TJ}CCS_{N2}$ values (222.7 and 222.0 Å^2 for $Mo_6O_{19}^{2-}$ and $W_6O_{19}^{2-}$ and 336.0 and 334.4 Å^2 for $PMo_{12}O_{40}^{3-}$ and $PW_{12}O_{40}^{3-}$) were within less than 2% relative error, confirming the validity of these LJ parameters for Mo-N_2 and W-N_2 interactions.

CONCLUSIONS

The collision cross sections of bare Lindqvist and Keggin polyoxometalates anions with Mo and W atoms were determined and found to be reproducible with different experimental settings before and after the ion mobility cell. Their $^{DT}CCS_{N2}$ values were consistent with earlier measurements on a TOFWerk instrument and the $^{DT}CCS_{He}$ values of Lindqvist ions were consistent with previously published values. Discrepancies for the ^{DT}CCS of bare Keggin ion $PW_{12}O_{40}^{3-}$ and for clusters of POMs with TBA ions remain unexplained, but we hypothesize that partially solvated anions still present upon entering the ion mobility cell could shift drift times to higher values. Effective temperature at high fields may also play a role for these multiply charged ions: high fields are expected to decrease CCS values. The fact that POMs of similar structures and very different masses exhibited similar CCS values both in He and N_2, although expected, is uncommon in ion mobility experiments. The existence of such ions of different masses and well-defined rigid structures could constitute attractive calibrants or model systems to test velocity relaxation effects in travelling wave ion mobility.[64,65] Finally, Lennard-Jones parameters for Mo and W interactions with He and N_2 determined herein are similar for both metals of the 6th group of the periodic table. The proposed values yielded relative errors of 2% or less on collision cross sections calculated with the trajectory method for bare Lindqvist and Keggin anions. These values would need to be further tested on different temperatures and ions, but constitute a first set to interpret POM molecular structures based on experimental CCS values.

Acknowledgments

The authors gratefully acknowledge Normandie Université (NU), the Région Normandie, the Centre National de la Recherche Scientifique (CNRS), Université de Rouen Normandie (URN), INSA Rouen Normandie, Innovation Chimie Carnot (I2C), the Labex SynOrg (ANR-11-LABX-0029), the graduate school for research Xl-Chem (ANR-18-EURE-0020 XL CHEM, the European Regional Development Fund (ERDF) Nº HN0001343 for financial support and the Centre Régional Informatique et d'Applications Numériques de Normandie (CRIANN) for computational time (N°2013005).

Conflicts of interest

There are no conflicts to declare.

Notes and references

1 L. Cronin and A. Muller, *Chem Soc Rev*, 2012, **41**, 7333-7334.
2 D. E. Katsoulis, *Chem Rev*, 1998, **98**, 359-388.
3 J. Y. Pope M., Fournier M., *Heteropoly and Isopoly Oxometalates*, Springer, Berlin, 1983.
4 C. Dablemont, A. Proust, R. Thouvenot, C. Afonso, F. Fournier and J. C. Tabet, *Inorg Chem*, 2004, **43**, 3514-3520.
5 T.-C. Lau, J. Wang, R. Guevremont and K. W. M. Siu, *J. Chem. Soc., Chem. Commun.*, 1995, DOI: 10.1039/c39950000877.
6 C. R. Mayer, C. Roch-Marchal, H. Lavanant, R. Thouvenot, N. Sellier, J. C. Blais and F. Secheresse, *Chemistry*, 2004, **10**, 5517-5523.
7 H. N. Miras, E. F. Wilson and L. Cronin, *Chem Commun (Camb)*, 2009, DOI: 10.1039/b819534j, 1297-1311.
8 M. Piot, S. Hupin, H. Lavanant, C. Afonso, L. Bouteiller, A. Proust and G. Izzet, *Inorg Chem*, 2017, **56**, 8490-8496.
9 Y. F. Song, D. L. Long, S. E. Kelly and L. Cronin, *Inorg Chem*, 2008, **47**, 9137-9139.
10 A. J. Surman, P. J. Robbins, J. Ujma, Q. Zheng, P. E. Barran and L. Cronin, *J Am Chem Soc*, 2016, **138**, 3824-3830.
11 S. Hupin, H. Lavanant, S. Renaudineau, A. Proust, G. Izzet, M. Groessl and C. Afonso, *Rapid Commun Mass Spectrom*, 2018, **32**, 1703-1710.

12 G. Izzet, A. Macdonell, C. Rinfray, M. Piot, S. Renaudineau, E. Derat, B. Abecassis, C. Afonso and A. Proust, *Chemistry*, 2015, **21**, 19010-19015.
13 M. Marianski, J. Seo, E. Mucha, D. A. Thomas, S. Jung, R. Schlögl, G. Meijer, A. Trunschke and G. von Helden, *J. Phys. Chem. C*, 2018, **123**, 7845-7853.
14 J. Thiel, D. Yang, M. H. Rosnes, X. Liu, C. Yvon, S. E. Kelly, Y. F. Song, D. L. Long and L. Cronin, *Angew Chem Int Ed Engl*, 2011, **50**, 8871-8875.
15 D. P. Smith, T. W. Knapman, I. Campuzano, R. W. Malham, J. T. Berryman, S. E. Radford and A. E. Ashcroft, *Eur J Mass Spectrom (Chichester)*, 2009, **15**, 113-130.
16 J. A. Picache, B. S. Rose, A. Balinski, K. L. Leaptrot, S. D. Sherrod, J. C. May and J. A. McLean, *Chem Sci*, 2019, **10**, 983-993.
17 17J. G. Forsythe, A. S. Petrov, C. A. Walker, S. J. Allen, J. S. Pellissier, M. F. Bush, N. V. Hud and F. M. Fernandez, *Analyst*, 2015, **140**, 6853-6861.
18 J. Hofmann, W. B. Struwe, C. A. Scarff, J. H. Scrivens, D. J. Harvey and K. Pagel, *Anal Chem*, 2014, **86**, 10789-10795.
19 K. M. Hines, J. C. May, J. A. McLean and L. Xu, *Anal Chem*, 2016, **88**, 7329-7336.
20 C. S. Hoaglund, Y. Liu, A. D. Ellington, M. Pagel and D. E. Clemmer, *J. Am. Chem. Soc.*, 1997, **119**, 9051-9052.
21 A. Marchand, S. Livet, F. Rosu and V. Gabelica, *Anal Chem*, 2017, **89**, 12674-12681.
22 D. E. Clemmer, Collision cross sections (in Å2) of individual protein charge states, https://clemlab.sitehost.iu.edu/Research/Cross%20Section%20Database/Proteins/protein_cs.htm, 2021).
23 H. Lavanant, M. Groessl and C. Afonso, *Int. J. Mass Spectrom.*, 2019, **442**, 14-22.
24 24X. Lopez, J. J. Carbo, C. Bo and J. M. Poblet, *Chem Soc Rev*, 2012, **41**, 7537-7571.
25 E. Broclawik, *International Journal of Quantum Chemistry*, 1995, **56**, 779-785.
26 R. Moriyama, R. Sato, M. Nakano, K. Ohshimo and F. Misaizu, *J Phys Chem A*, 2017, **121**, 5605-5613.
27 L. Vila-Nadal, E. F. Wilson, H. N. Miras, A. Rodriguez-Fortea, L. Cronin and J. M. Poblet, *Inorg Chem*, 2011, **50**, 7811-7819.
28 G. von Helden, M. T. Hsu, N. Gotts and M. T. Bowers, *J. Phys. Chem.*, 2002, **97**, 8182-8192.
29 S. E. Anderson, C. Bleiholder, E. R. Brocker, P. J. Stang and M. T. Bowers, *Int. J. Mass Spectrom.*, 2012, **330-332**, 78-84.
30 A. A. Shvartsburg and M. F. Jarrold, *Chem. Phys. Lett.*, 1996, **261**, 86-91.
31 M. F. Mesleh, J. M. Hunter, A. A. Shvartsburg, G. C. Schatz and M. F. Jarrold, *J. Phys. Chem.*, 1996, **100**, 16082-16086.
32 C. Larriba and C. J. Hogan, *J. Comput. Phys.*, 2013, **251**, 344-363.
33 I. Campuzano, M. F. Bush, C. V. Robinson, C. Beaumont, K. Richardson, H. Kim and H. I. Kim, *Anal. Chem.*, 2012, **84**, 1026-1033.
34 P. M. Lalli, Y. E. Corilo, M. Fasciotti, M. F. Riccio, G. F. de Sá, R. J. Daroda, G. H. M. F. Souza, M. McCullagh, M. D. Bartberger, M. N. Eberlin and I. Campuzano, *J. Mass Spectrom.*, 2013, **48**, i-i.
35 C. K. Siu, Y. Guo, I. S. Saminathan, A. C. Hopkinson and K. W. Siu, *J Phys Chem B*, 2010, **114**, 1204-1212.
36 R. Contant, W. G. Klemperer and O. Yaghi, in *Inorg. Synth.*, 1990, DOI: https://doi.org/10.1002/9780470132586.ch18, pp. 104-111.
37 W. G. Klemperer, in *Inorg. Synth.*, 1990, DOI: https://doi.org/10.1002/9780470132586.ch15, pp. 74-85.
38 R. Thouvenot, M. Fournier, R. Franck and C. Rocchiccioli-Deltcheff, *Inorg Chem*, 2002, **23**, 598-605.
39 H. Weiner, J. D. Aiken and R. G. Finke, *Inorg Chem*, 1996, **35**, 7905-7913.
40 J. C. May, C. R. Goodwin, N. M. Lareau, K. L. Leaptrot, C. B. Morris, R. T. Kurulugama, A. Mordehai, C. Klein, W. Barry, E. Darland, G. Overney, K. Imatani, G. C. Stafford, J. C. Fjeldsted and J. A. McLean, *Anal Chem*, 2014, **86**, 2107-2116.
41 S. M. Stow, T. J. Causon, X. Zheng, R. T. Kurulugama, T. Mairinger, J. C. May, E. E. Rennie, E. S. Baker, R. D. Smith, J. A. McLean, S. Hann and J. C. Fjeldsted, *Anal Chem*, 2017, **89**, 9048-9055.
42 V. Gabelica, S. Livet and F. Rosu, *J Am Soc Mass Spectrom*, 2018, **29**, 2189-2198.
43 D. A. Polasky, S. M. Dixit, S. M. Fantin and B. T. Ruotolo, *Anal Chem*, 2019, **91**, 3147-3155.
44 M. Strohalm, M. Hassman, B. Kosata and M. Kodicek, *Rapid Commun Mass Spectrom*, 2008, **22**, 905-908.
45 M. Strohalm, D. Kavan, P. Novak, M. Volny and V. Havlicek, *Anal Chem*, 2010, **82**, 4648-4651.
46 H. E. Revercomb and E. A. Mason, *Analytical Chemistry*, 1975, **47**, 970-983.
47 J. Tucher, Y. Wu, L. C. Nye, I. Ivanovic-Burmazovic, M. M. Khusniyarov and C. Streb, *Dalton Trans*, 2012, **41**, 9938-9943.
48 J. Fuchs, W. Freiwald and H. Hartl, *Acta Crystallogr. Sect. B*, 1978, **34**, 1764-1770.
49 Y.-N. J. Dong-Bin Dang, Yan Bai, Xiao-Jing Pan, Jing-Ping Wang, *Journal*, 2010, DOI: 10.5517/ccpqq58.
50 C. P. P. D.Gabb, T.Boyd, S.G.Mitchell, H.N.Miras, De-Liang Long, L.Cronin, *Journal*, 2013, DOI: 10.5517/ccyxfhr.
51 D. Gabb, C. P. Pradeep, T. Boyd, S. G. Mitchell, H. N. Miras, D.-L. Long and L. Cronin, *Polyhedron*, 2013, **52**, 159-164.
52 M. J. Frisch, G. W. Trucks, H. B. Schlegel, G. E. Scuseria, M. A. Robb, J. R. Cheeseman, G. Scalmani, V. Barone, B. Mennucci, G. A. Petersson, H. Nakatsuji, M. Caricato, X. Li, H. P. Hratchian, A. F. Izmaylov, J. Bloino, G. Zheng, J. L. Sonnenberg, M. Hada, M. Ehara, K. Toyota, R. Fukuda, J. Hasegawa, M. Ishida, T. Nakajima, Y. Honda, O. Kitao, H. Nakai, T. Vreven, J. A. Montgomery. Jr, J. E. Peralta, F. Ogliaro, M. Bearpark, J. J. Heyd, E. Brothers, K. N. Kudin, V. N. Staroverov, R. Kobayashi, J. Normand, K. Raghavachari, A. Rendell, J. C. Burant, S. S. Iyengar, J. Tomasi, M. Cossi, N. Rega, N. J. Millam, M. Klene, J. E. Knox, J. B. Cross, V. Bakken, C. Adamo, J. Jaramillo, R. Gomperts, R. E. Stratmann, O. Yazyev, A. J. Austin, R. Cammi, C. Pomelli, J. W. Ochterski, R. L. Martin, K. Morokuma, V. G. Zakrzewski,

G. A. Voth, P. Salvador, J. J. Dannenberg, S. Dapprich, A. D. Daniels, Ö. Farkas, J. B. Foresman, J. V. Ortiz, J. Cioslowski and D. J. Fox, *Journal*, 2009.
53 J. D. Chai and M. Head-Gordon, *Phys. Chem. Chem. Phys.*, 2008, **10**, 6615-6620.
54 H. Hu, Z. Lu and W. Yang, *J Chem Theory Comput*, 2007, **3**, 1004-1013.
55 V. Shrivastav, M. Nahin, C. J. Hogan and C. Larriba-Andaluz, *J Am Soc Mass Spectrom*, 2017, **28**, 1540-1551.
56 J. Coots, V. Gandhi, T. Onakoya, X. Chen and C. Larriba-Andaluz, *J. Aerosol Sci*, 2020, **147**.
57 C. Larriba-Andaluz, J. Fernández-García, M. A. Ewing, C. J. Hogan and D. E. Clemmer, *Phys. Chem. Chem. Phys.*, 2015, **17**, 15019-15029.
58 J. Rus, D. Moro, J. A. Sillero, J. Royuela, A. Casado, F. Estevez-Molinero and J. Fernández de la Mora, *Int. J. Mass Spectrom.*, 2010, **298**, 30-40.
59 H. Ouyang, C. Larriba-Andaluz, D. R. Oberreit and C. J. Hogan, Jr., *J Am Soc Mass Spectrom*, 2013, **24**, 1833-1847.
60 C. J. Hogan, Jr. and J. Fernandez de la Mora, *Phys. Chem. Chem. Phys.*, 2009, **11**, 8079-8090.
61 F. A. Fernandez-Lima, C. Becker, K. Gillig, W. K. Russell, M. A. C. Nascimento and D. H. Russell, *J. Phys. Chem. A*, 2008, **112**, 11061-11066.
62 W. Humphrey, A. Dalke and K. Schulten, *Journal of Molecular Graphics*, 1996, **14**, 33-38.
63 A. K. Rappe, C. J. Casewit, K. S. Colwell, W. A. Goddard and W. M. Skiff, *J. Am. Chem. Soc.*, 1992, **114**, 10024-10035.
64 T. Wu, J. Derrick, M. Nahin, X. Chen and C. Larriba-Andaluz, *J Chem Phys*, 2018, **148**, 074102.
65 K. Richardson, D. Langridge, S. M. Dixit and B. T. Ruotolo, *Anal Chem*, 2021, **93**, 3542-3550.